



Growth and treatment of hydrogenated amorphous carbon nanoparticles in a low-pressure plasma

Oguz Han Asnaz¹  | Niklas Kohlmann² | Hauke Folger¹ | Franko Greiner¹ | Jan Benedikt¹ 

¹Institute of Experimental and Applied Physics, Kiel University, Kiel, Germany

²Faculty of Engineering, Kiel University, Kiel, Germany

Correspondence

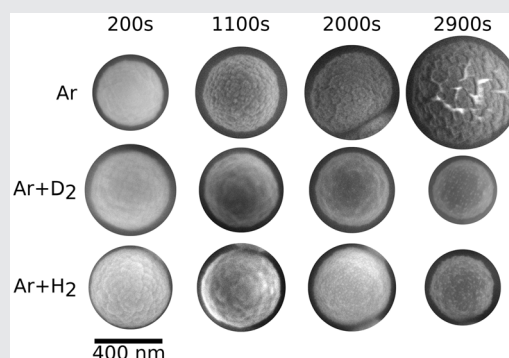
Oguz Han Asnaz, Institute of Experimental and Applied Physics, Kiel University, 24098 Kiel, Germany.
Email: asnaz@physik.uni-kiel.de

Funding information

Deutscher Akademischer Austauschdienst, Grant/Award Number: 57449433; Deutsche Forschungsgemeinschaft, Grant/Award Number: 411452476

Abstract

A parallel-plate, low-pressure plasma for fundamental nanodusty plasma research is used to grow hydrogenated amorphous carbon nanoparticles using an argon-acetylene gas mixture. The particles stay confined in the volume of the argon plasma after turning off the C₂H₂ gas flow and the effects of prolonged treatment with noble gas (Ar) and reactive gas mixtures (Ar/H₂, Ar/D₂, or Ar/O₂) are investigated using in situ infrared absorption spectroscopy. Additionally, ex situ scanning electron microscopy imaging of extracted nanoparticles is used to analyze their size and surface morphology. In 45 min of argon treatment, a size increase of about 50% is seen together with a decrease in sp² CH_x bonds and an increase in C=O bonds, indicating incorporation of oxygen from gas impurities into the particle material. All reactive gas mixtures lead to the expected etching of the nanoparticle material without any exchange reactions between gas-phase deuterium and surface-bonded hydrogen atoms. These results are important for in situ studies of nanoparticle clouds such as dust density wave diagnostics, but they also provide fundamental information about plasma interaction with a-C:H material.



KEYWORDS

FTIR, infrared absorption spectroscopy (IRAS), low-pressure discharges, particles, surface modification

This is an open access article under the terms of the Creative Commons Attribution-NonCommercial License, which permits use, distribution and reproduction in any medium, provided the original work is properly cited and is not used for commercial purposes.

© 2022 The Authors. *Plasma Processes and Polymers* published by Wiley-VCH GmbH.

1 | INTRODUCTION

The plasma-surface boundary is a multifaceted region with many relevant interactions happening between different species. There are charging effects due to ion and electron fluxes from the plasma as well as secondary electrons being emitted from the surface. High-energy electrons and UV radiation in the plasma can trigger surface reactions and allow chemical reactions that are usually only seen in high-temperature chemistry. Under these conditions, it is possible to use reactive gasses for the production of hydrocarbon materials used in many applications. While initially seen as a negative side effect,^[1,2] nanoparticle formation in these reactive plasmas has found many applications in both industrial topics^[3] as well as fundamental research.^[4–6]

One such fundamental research area is the field of nanodusty plasmas, where high particle densities lead to the creation of an electron-depleted two species plasma of ions and dust particles.^[7–9] These systems have been the main focus of works investigating dust formation processes^[10,11] as well as the resulting phenomena like dust density waves^[9,12] and cyclic, layered growth.^[13,14] The setups used in these works are typically not built for ultrahigh vacuum and have small, technically unavoidable leaks of ambient air. In experiments requiring long-term confinement of particles, these have led to oxidation effects changing the particle properties, such as size, surface morphology, and probably also composition or surface passivation over time.^[15–18]

In this study, a multipass white cell for in situ Fourier transform infrared absorption spectroscopy (FTIR) was integrated into a plasma setup, previously used for fundamental nanodusty plasma research, and is used to characterize the effects of gas impurities on the nanoparticles confined in a low-pressure discharge. After their generation in the Ar/C₂H₂ plasma, the particles are left confined either in the argon-only plasma (plus gas impurities) or in an argon plasma with a small addition of a reactive gas (oxygen, hydrogen, or deuterium) for comparison. We call this part of the experiment a “treatment” in this article. Additionally, particles are extracted several times during the very same treatment process in which the corresponding FTIR measurements take place, using an electrostatic particle extractor (EPEX)^[19] to analyze ex situ their size and surface morphology changes with scanning electron microscopy (SEM).

2 | EXPERIMENTAL SETUP AND DIAGNOSTICS

The plasma system used in this study has previously been used for various dusty plasma experiments studying in situ particle growth.^[20] It consists of a capacitively

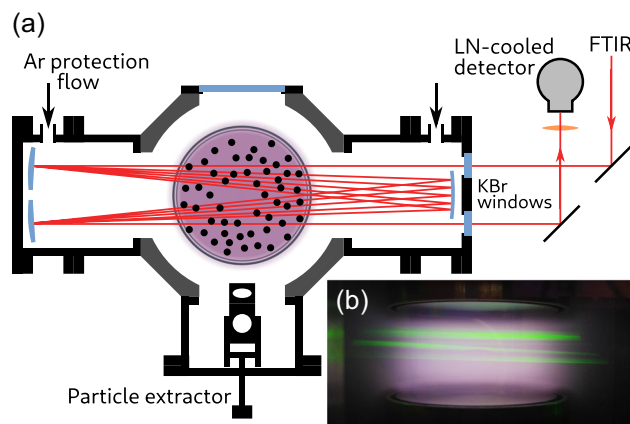


FIGURE 1 (a) Top-view of the plasma setup. Electrodes and their Faraday shields are shown as circles in the center. The IR beam is coupled in through KBr windows with a multipass setup for a longer optical path before being measured by the liquid nitrogen cooled detector. On the second axis, an electrostatic particle extractor is placed for sample extraction. (b) Side-view into the plasma chamber containing a nanodusty plasma. The IR beam was replaced by a green laser to visualize the beam path using scattered light from the particles

coupled parallel plate discharge operated at 13.56 MHz. In this study, a comparatively low RF power of 5 W is used to slow down particle growth. The stainless-steel electrodes with a diameter of 60 mm and a vertical gap of 30 mm are surrounded by a grounded Faraday shield. They are driven in a push-pull mode using a balun. There are four lateral access ports: two to facilitate a multipass infrared (IR) setup, one to introduce an EPEX, and one for a window for optical access.

The IR-spectrometric monitoring is done using a commercial FTIR spectrometer (Bruker Vertex 80v), which is coupled through KBr windows into a white cell (neoplas control GmbH) for up to 20 passes, increasing the optical path through the dust cloud to $z \approx 20 \cdot 60 \text{ mm} = 1.2 \text{ m}$. Figure 1 shows the scheme of the setup and the photograph of the green light used in place of the IR light to visualize the light path through the light scattering on the particles in the dust cloud. In the studied diameter regime, nanoparticles are distributed homogeneously through the plasma volume due to their negligible weight except for the small particle-free void in the plasma center (see the scattered light in Figure 1b or the images of the scattered laser light in our previous publications^[4,9]). The beam entering the White cell has a diameter of about 2 mm and over multiple reflections passes through a 1 cm high and 4 cm wide region in the upper half of the electrode gap. For higher temporal resolution, the rapid scan option of the FTIR spectrometer is used in conjunction with an optical long-pass filter for $k \geq 3900 \text{ cm}^{-1}$ avoiding aliasing effects. This

allows measuring IR absorption spectra at a resolution of 2 cm^{-1} at 10 Hz. During the particle growth, 64 scans are averaged to one data point, whereas during the particle confinement 512 scans are used for greater noise reduction.

Deposition on the aluminium-coated mirrors is prevented by placing the argon inlets between mirrors and the plasma chamber to act as a gas curtain. The reactive gasses acetylene (C_2H_2), oxygen, hydrogen, and deuterium are introduced via a separate inlet on the top of the chamber. The entire beam path from the FTIR to the plasma chamber is enclosed and flushed with nitrogen to minimize absorption lines from CO_2 and water vapor in the ambient air. An argon flow rate of 6.4 sccm with 1.6 sccm of C_2H_2 (20% admixture) at a gas pressure of 22 Pa is used for particle growth. After turning off the acetylene admixture, the pressure drops to 18 Pa. The treatment gas is added at a flow rate of 0.5 sccm for H_2 and D_2 and 0.8 sccm for O_2 .

Particles are extracted from the cloud onto $1 \times 1\text{ cm}$ silicon wafers during the treatment process using an EPEX.^[19] The collection is performed through the application of a short voltage pulse of 170 V for only 200 ms without disturbing the system significantly. EPEX is constructed with eight wafer holders on a rotating carousel enabling the consecutive extraction of eight samples without breaking the vacuum.

These samples were imaged using a Zeiss Supra 55 V scanning electron microscope (SEM) to measure the particle's size and surface structure. To maximize information of the surface structure the penetration depth of the impinging electrons needs to be as low as possible. Therefore, the acceleration voltage was lowered down to 500 V in combination with low working distances and utilizing the GEMINI in-lens-detector for the highest resolution measurements. By utilizing low voltage SEM, charging effects occurring due to the insulating nature of the particles as well as beam damage are minimized likewise.^[21–23] Thus, high-resolution imaging of the surface structure of the particles is possible without further coating of the samples.

The measurement procedure begins with flushing the chamber with the argon/acetylene gas mixture. At $t = 0\text{ s}$ the plasma is switched on and the growth process takes place for 90 s until the acetylene supply is turned off. The transition from Ar/ C_2H_2 plasma at 22 Pa to argon plasma at 18 Pa is smooth without the loss of particle confinement or any other change of particle properties. After letting the system settle for 2 min, the first sample is extracted and the prolonged particle treatment through the plasma, either in argon gas only or with the reactive gas (H_2 , D_2 , or O_2), starts. Three further particle samples are extracted every 15 min. There were no samples

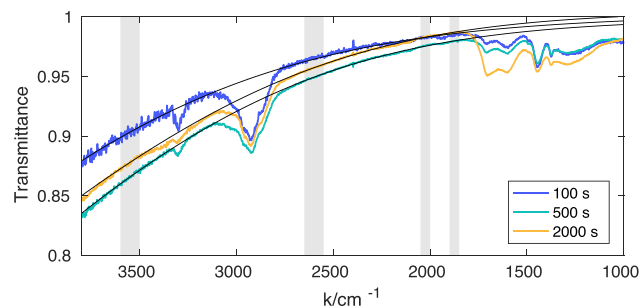


FIGURE 2 Normalized transmission spectra of confined a-C:H nanoparticles without additional treatment. In black, the corresponding background fits are shown, which were fitted to the area marked with gray boxes

extracted for the Ar/ O_2 treatment with very fast particle etching.

The IR transmission spectra are measured relative to the reference spectrum obtained in an evacuated chamber without a gas flow before each measurement cycle. They show two separate sources of absorption. First, a broad background transmission reduction due to light scattering is observed on the nanoparticles with increasing intensity towards higher wavenumbers. Second, vibrational excitation with narrower absorption bands is present in several positions in the spectra. The broad background is fitted to a Mie scattering model^[27] at manually selected regions without absorption bands using particle diameter d as a free parameter and subsequently subtracted from the spectra (see Figure 2). The decomposition of the resulting absorption spectrum is done using Gaussian functions for each absorption peak representing a vibrational excitation mode of a specific chemical bond. Additionally, a linear background is used in the region around 1500 cm^{-1} to fit the data. The used parameters together with references to the original works are shown in Table 1. The resulting spectra with an exemplary decomposition for argon plasma-treated particles are shown in Figure 3. The integrated intensities of the absorbing features are converted into bond concentrations using the known optical path length and calibration factors given by Wexler.^[26]

3 | RESULTS

3.1 | Long-term nanoparticle confinement in argon plasma

The plasma setup described above is typically used in dusty plasma experiments involving confined particles. Previous works with both microparticles^[15–17,28] and

nanoparticles^[18] report a loss of particle mass occurring either from small oxygen leaks leading to etching processes or impinging ions leading to melting-like processes on the particle surface.^[29] Against these expectations, the SEM measurements shown in Figure 4 present a clear increase in particle size for the argon-treated case. After 45 min of plasma exposure, the particle radius increases by 50% and different, larger scale surface features compared to the typical cauliflower-like structure of untreated particles appear on their surface.

TABLE 1 Used parameters for Gaussian line fits

Excitation mode	$\bar{\nu}/\text{cm}^{-1}$	σ/cm^{-1}	References
sp ² CH ₂ olef. asym.	3085	20	[24]
sp ² CH arom.	3035	23	[24]
sp ² CH olef. sym.	3000	16	[24]
sp ² CH ₂ olef. sym.	2975	18	[24]
sp ³ CH ₃ asym.	2955	20	[24]
sp ³ CH, sp ³ CH ₂ asym.	2920	16	[24]
sp ³ CH ₃ sym.	2885	28	[24]
sp ³ CH ₂ sym.	2855	40	[24]
H-bonded O–H	3320	100	[25]
C=O	1710	25	[26]
Cyclic C=O	1670	13	[26]

Note: Wavenumbers were taken from the given reference. Peak widths are fitted to the measured curves. Symmetric (sym.), asymmetric (asym.), olefinic (olef.), and aromatic (arom.) vibrations are labeled.

The infrared spectra show that sp² and sp³ CH bonds evolve differently over time after the initial stage of particle nucleation and growth in the C₂H₂ plasma (see Figure 5a). While sp³-hybridized bonds slightly increase over time, a decrease in sp² bonds is seen together with an increase in C=O and O–H bonds. This indicates that oxygen is primarily attaching at the sp² C sites instead of performing an etching process, explaining the particle size increase with an oxygen enrichment of the material. We cannot, however, distinguish between the growth of an oxide layer on top of the particle, oxygen diffusion into the particle bulk, and oxidation reactions in the whole particle volume. The large diameter increase together with the changing surface features suggests bulk addition is taking place as well. The small increase of the sp³ CH₃ absorption may stem from an increase in surface area, leading to more methyl groups at the end of the polymeric chains.

The increase of the particle volume can be used to estimate the absolute flux of O atoms to the surface necessary to achieve the particle growth in 45 min of the plasma exposure. Assuming the constant material density of 1 g cm⁻³ (typical value for polymer-like a-C:H films^[31]) for both a-C:H and oxidized a-C:H material and calculating the volume change of the particle (change of a from 400 to 600 nm) the number of O atoms reacting at each particle during the process can be estimated to be around 1 × 10⁶ O atoms/particle/s. This estimation is in good agreement with the measured concentrations of sp² CO and H-bonded O–H groups (see Figure 5a), which give us a similar flux of 1.3 × 10⁵ O atoms/particle/s deposited in these bonds.

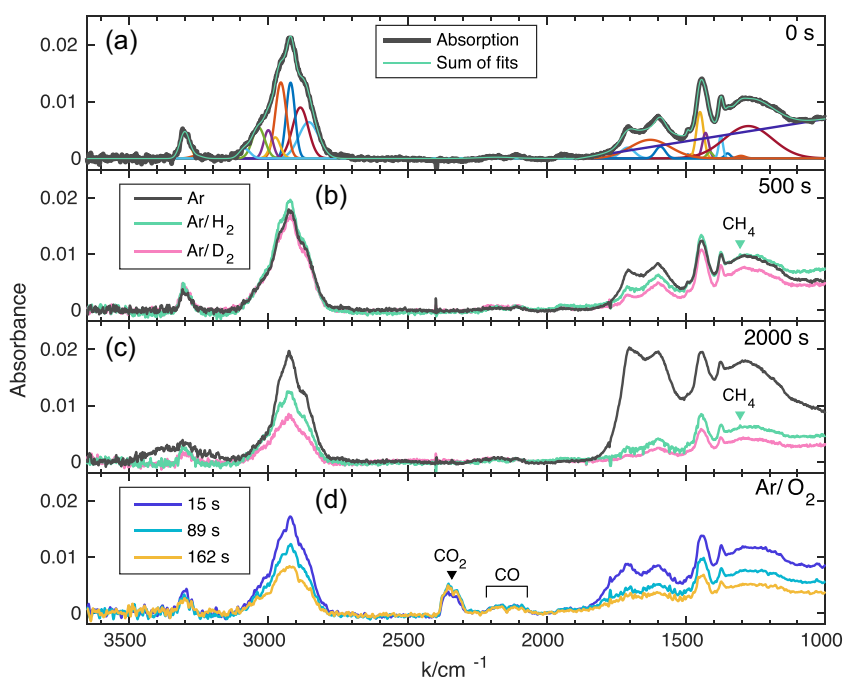


FIGURE 3 Infrared transmission spectra adjusted for background. (a) Decomposition into different excitation modes for argon-treated sample shortly after particle generation. (b,c) Spectra after 500 and 2000 s of treatment. The position of the CH₄ fundamental bending mode was marked. (d) Spectra from O₂ treatment over 162 s of treatment. The positions of the CO₂ asymmetric stretching mode and the ro-vibrational CO band are marked

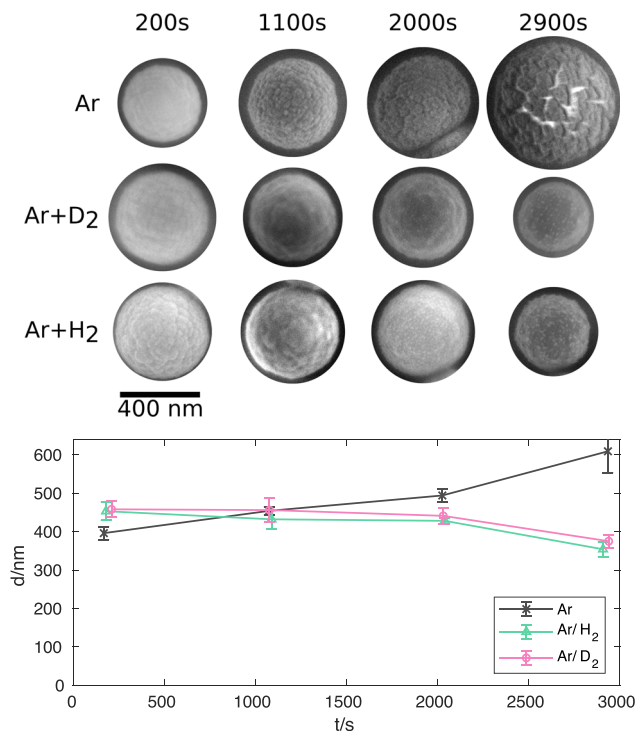


FIGURE 4 Scanning electron microscopy images of the extracted particle samples and resulting temporal size evolution in the case of Ar, Ar/H₂, and Ar/D₂ treatment, respectively. The time above the particles indicates the length of the treatment. Error bars were gained from measuring particle radii on overview images of 20–80 particles

This flux can be realized as a collision rate of neutral gas impurities with the particles, where the impurity partial pressure is at a level of approximately 4×10^{-4} Pa (assuming a gas temperature around 300 K). This is below the base pressure of the reactor ($\approx 10^{-2}$ Pa), but the impurities will react at the particle surface with a probability lower than 100%, explaining the difference.

Another source of the O flux can be the ion flux to the particles due to plasma ionized impurities (O_2^+ , O^+ , H_2O^+ , ...). The particle charge is limited due to strong electron depletion in this discharge due to the Havnes effect,^[9] where the orbital motion limited charge on an isolated particle in the same plasma would be roughly 80 times larger. Estimating the collision rate based on the Coulomb interaction and particle diameter of 500 nm and particle charge of 20 elementary charges, an ion impurity density in the order of 6×10^6 cm⁻³ is needed to explain the O flux, again smaller than the plasma density of approximately 10^9 cm⁻³, measured by Tadsen et al.^[9] These calculations show that probably both neutral and ionized impurities contribute to the particle oxidation process.

The last possibility of particle growth could be the sputtering of a-C:H:O material from the discharge electrodes, which is also formed in the interaction of impurities with the a-C:H film deposited there during the Ar/C₂H₂ plasma and which can redeposit on the particles. However, the high gas pressure of 18 Pa and low absorbed power with low peak-to-peak voltage results in a collision-dominated sheath with low ion energy at the electrodes and we expect that similar processes will take place both at the electrode and particle surfaces, without any physical sputtering of the material at the electrode surface. Additionally, the electrode and reactor wall surfaces covered by the thin a-C:H film will bond oxygen-containing species from the gas phase and, therefore, reduce the level of oxygen-containing impurities to a lower value compared to a reactor with clean stainless-steel surfaces, providing a possible explanation, why the otherwise observed etching in other experiments with large externally injected particles is not present in our case.

3.2 | Nanoparticles in Ar/O₂ plasma

The experiment was repeated with a 12% oxygen admixture after the growth process to test the effect of the large excess of O₂ on the particle growth/etching and its properties. Particles are etched quickly under these conditions, where the IR absorption disappears completely after about 5 min. This etching rate is about 20 times higher than under conditions with H₂ or D₂ (see later) as determined from the change of the fitted Mie background absorption. Regarding the fast etching rate, no attempt has been performed to extract the particles during the Ar/O₂ plasma etching and only the IR absorption has been followed. However, no increase in C=O or O–H bonds has been observed contrary to the argon plasma treatment. Rather, strong CO₂ and weak H₂O molecular absorption lines appear in the spectra indicating the presence of these etching products in the gas phase. Therefore, the oxygen enrichment process seen in the argon treatment case only happens at very low impurity (O₂, H₂O) concentrations as estimated above, while a much faster etching process occurs at high O₂ concentrations. Whether a-C:H particles or particles from other materials such as melamine formaldehyde (MF) or polymethylmethacrylate (PMMA) will grow due to fixation of oxygen or be etched on the time-scale of hours will very probably depend on the level of oxygen-containing gas impurities in the particular setup and can explain the observed reduction of the size of micrometer particles in other argon plasmas.^[17,28]

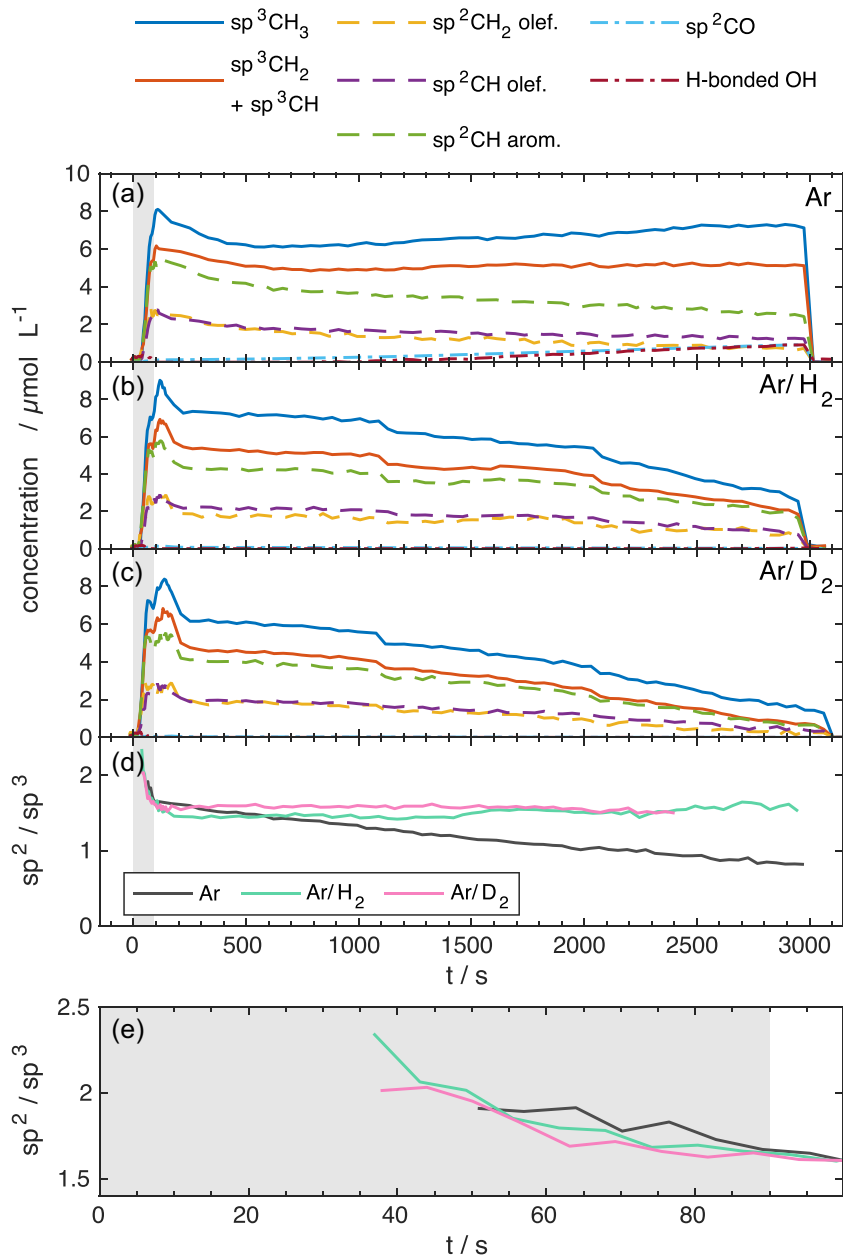


FIGURE 5 (a–c) Time evolution of CH bond concentrations determined by decomposition of the stretching vibrations in the case of Ar, Ar/H₂, and Ar/D₂ treatment, respectively. Absorption line intensities were converted using calibration factors described by Ristein et al.^[30] The particle growth period is marked in gray. (d,e) The ratio of sp² to sp³ C sites for different treatments with an enlarged version of the first 100 s

3.3 | Nanoparticles in Ar/H₂ and Ar/D₂ plasma

Admixing 0.5 sccm of hydrogen to the argon gas after the growth process and comparison to the same experiment with deuterium provides information about an etching of the a-C:H nanoparticles under these conditions and possible hydrogen exchange reactions at the nanoparticle surface visible as possible appearance of C–D bonds and disappearance of C–H bonds in the absorption spectra. SEM imaging shows a particle radius decrease of 20% after 45 min together with a substantial change in surface structure, where the typical cauliflower structure is replaced by a seemingly smoother surface with many small features on top of it.

The material etching is also visible in the infrared spectrum with a general decrease in absorption strength over time. Here, the absorption of all C–H bonds evolves equally with a constant ratio of sp² to sp³ bonds (see Figure 5d), in contrast to the linear decrease of this ratio in the case of argon treatment due to the previously described incorporation of oxygen from impurities into the material. It can be assumed that the Ar/H₂ plasma treatment leads to etching as well as reduction of oxygen, stopping the oxidation of the particles. Atomic hydrogen and hydrogen ions (H⁺, H₂⁺, H₃⁺) are the probable reactive species at the nanoparticle surface. Typical etch products resulting from the interaction of hydrogen-containing plasma with a-C:H films are CH₄ and C₂H₄ molecules,^[10] where weak absorption due to the Q-branch of the ν₄

fundamental bending mode of the CH_4 molecule at around 1306 cm^{-1} , the most dominant CH_4 absorption feature in this spectral range,^[32] is observed during the Ar/ H_2 plasma treatment.

To check for hydrogen exchange processes at the nanoparticle surface, the same procedure was repeated with deuterium. The exchange of C–H bonds with C–D bonds should lead to additional absorption peaks around 2100 cm^{-1} from CD_n stretching modes^[33] and to the reduction of C–H absorption. These changes were not observed at any time during the treatment, indicating that etching is the predominant process of hydrogen interaction with the nanoparticles in Ar/ H_2 plasma.

3.4 | Particle growth phase

The infrared spectra first show a signal above the noise level at about $t = 40\text{ s}$, which corresponds to a particle diameter of 220 nm. The spectral decomposition shows a much higher sp^2 to sp^3 CH bond ratio at this point with values of about 1.1, which decrease to about 0.8 in the next 50 s (see Figure 5e).

Kovačević et al. describe sp^2 -poor material being formed during the surface growth phase of carbon particles synthesized from acetylene,^[34] which sets on after a diameter of about 10 nm. Annealing processes by surface heating can increase the sp^2 content of particles and might explain the observed higher initial ratio in our experiment as selective heating mechanisms are more efficient for smaller particles.

4 | CONCLUSION

The changes of chemical composition, size, and surface morphology of a-C:H particles in prolonged treatment in argon plasma and argon plasma with an admixture of oxygen, hydrogen, and deuterium have been studied in situ and ex situ. In situ IR spectrometry reveals that oxygen-containing impurities in typical experimental setups used in nanodusty plasma research affect particles on longer time scales. However, the usual assumption of oxygen etching was not seen for our experimental conditions. Rather, at the used conditions, the particles' oxidation is observed, which led to a particle size increase and a significant change of surface morphology, where the cauliflower-like surface changed to show larger-scale structures.

Additionally, the analysis of the FTIR spectra showed a decrease of sp^2CH_x bonds together with an increase in C=O and O–H bonds, indicating preferential incorporation of oxygen at the carbon double

bonds. At higher concentrations, oxygen treatment showed a fast etching process with no incorporation of oxygen being visible in the infrared spectra. Treating the particles with hydrogen led to a pure etching process as well, without any exchange reactions of hydrogen at the particle surface. This was shown in additional measurements using deuterium as a treatment gas. Here, the particle size decreased over time with the change of the surface to morphology with a smaller scale structure.

To conclude, our experiments have shown that the level of gas impurities in argon gas, the usual gas used in nanodusty plasma experiments, influences the particle size as well as their other properties and that the resulting effect can be even the increase of nanoparticle diameter. The nanodusty plasma experiments with longer confinement times should be aware of this effect and should consider it in the evaluation of experimental data. Additionally, we have also shown that in situ multiple-pass White cell IR absorption spectroscopy can be effectively combined with nanoparticle extraction and further ex situ analysis, offering an effective tool for the study of fundamental processes in plasma interaction with a variety of plasma-confined nanoparticles generated from other precursors such as silane or from a mixture of several reactive gases.^[35–37]

ACKNOWLEDGMENTS

The authors thank the German Research Foundation (DFG, project 411452476) for funding this study, and O. H. A. and J. B. thank the German Academic Exchange Service (DAAD, project 57449433) for supporting this study through their people exchange program.

DATA AVAILABILITY STATEMENT

The data that support the findings of this study are available from the corresponding author upon reasonable request.

ORCID

Oguz Han Asnaz  <http://orcid.org/0000-0002-8133-4250>

Jan Benedikt  <http://orcid.org/0000-0002-8954-1908>

REFERENCES

- [1] G. S. Selwyn, J. Singh, R. S. Bennett, *J. Vac. Sci. Technol., A* **1989**, 7, 2758.
- [2] J. Winter, *Plasma Phys. Controlled Fusion* **2004**, 46, B583.
- [3] U. R. Kortshagen, R. M. Sankaran, R. N. Pereira, S. L. Girshick, J. J. Wu, E. S. Aydil, *Chem. Rev.* **2016**, 116, 11061.
- [4] F. Greiner, A. Melzer, B. Tadsen, S. Groth, C. Killer, F. Kirchschrager, F. Wieben, I. Pilch, H. Krüger, D. Block, A. Piel, S. Wolf, *Eur. Phys. J. D* **2018**, 72, 81.

- [5] H. Krüger, E. Sündermann, A. Melzer, *Plasma Sources Sci. Technol.* **2021**, *30*, 105005.
- [6] H. Krüger, E. Thiessen, F. X. Bronold, H. Fehske, A. Melzer, *Phys. Rev. E* **2021**, *104*, 045208.
- [7] O. Havnes, G. E. Morfill, C. K. Goertz, *J. Geophys. Res.* **1984**, *89*, 10999.
- [8] C. K. Goertz, *Rev. Geophys.* **1989**, *27*, 271.
- [9] B. Tadsen, F. Greiner, S. Groth, A. Piel, *Phys. Plasmas* **2015**, *22*, 113701.
- [10] J. Benedikt, *J. Phys. D. Appl. Phys.* **2010**, *43*, 043001.
- [11] E. Kovačević, I. Stefanović, J. Berndt, J. Winter, *J. Appl. Phys.* **2003**, *93*, 2924.
- [12] B. Tadsen, F. Greiner, A. Piel, *Phys. Rev. E* **2018**, *97*, 033203.
- [13] F. M. J. H. van de Wetering, R. J. C. Brooimans, S. Nijdam, J. Beckers, G. M. W. Kroesen, *J. Phys. D. Appl. Phys.* **2015**, *48*, 035204.
- [14] S. Groth, F. Greiner, A. Piel, *Plasma Sources Sci. Technol.* **2019**, *28*, 115016.
- [15] G. H. P. M. Swinkels, E. Stoffels, W. W. Stoffels, N. Simons, G. M. W. Kroesen, F. J. de Hoog, *Pure Appl. Chem.* **1998**, *70*, 1151.
- [16] J. Carstensen, H. Jung, F. Greiner, A. Piel, *Phys. Plasmas* **2011**, *18*, 033701.
- [17] O. H. Asnaz, H. Jung, F. Greiner, A. Piel, *Phys. Plasmas* **2017**, *24*, 083701.
- [18] S. Groth, F. Greiner, B. Tadsen, A. Piel, *J. Phys. D. Appl. Phys.* **2015**, *48*, 465203.
- [19] M. Dworschak, O. H. Asnaz, F. Greiner, *Plasma Sources Sci. Technol.* **2021**, *30*, 035011.
- [20] B. Tadsen, F. Greiner, A. Piel, *Phys. Plasmas* **2014**, *21*, 103704.
- [21] M. Nakagawa, S. Takeuchi, A. Muto, T. Ogashiwa, S. White, M. Sato, *Microsc. Microanal.* **2005**, *11*, 146.
- [22] A. Endo, M. Yamada, S. Kataoka, T. Sano, Y. Inagi, A. Miyaki, *Colloids Surfaces A Physicochem. Eng. Asp.* **2010**, *357*, 11.
- [23] S. Asahina, T. Togashi, O. Terasaki, *Microsc. Anal.* **2012**, *7*, 12.
- [24] J. Robertson, *Mater. Sci. Eng., R* **2002**, *37*, 129.
- [25] G. Socrates, *J. Raman Spectrosc.*, 3rd ed., John Wiley & Sons Ltd., Chichester **2001**, p. 347.
- [26] A. S. Wexler, *Appl. Spectrosc. Rev.* **1967**, *1*, 29.
- [27] H. C. van de Hulst, *Light Scattering by Small Particles*, Dover Publications Inc., New York **1981**.
- [28] N. Kohlmann, F. Wieben, O. H. Asnaz, D. Block, F. Greiner, *Phys. Plasmas* **2019**, *26*, 053701.
- [29] M. CollaudCoen, R. Lehmann, P. Groening, L. Schlapbach, *Appl. Surf. Sci.* **2003**, *207*, 276.
- [30] J. Ristein, R. T. Stief, L. Ley, W. Beyer, *J. Appl. Phys.* **1998**, *84*, 3836.
- [31] T. Schwarz-Selinger, A. vonKeudell, W. Jacob, *J. Appl. Phys.* **1999**, *86*, 3988.
- [32] P. Linstrom, W. Mallard, Eds., *NIST Chem. WebBook, NIST Stand. Ref. Database Number 69*, National Institute of Standards and Technology, Gaithersburg, MD, retrieved January 17, 2022.
- [33] A. vonKeudell, *Thin Solid Films* **2002**, *402*, 1.
- [34] E. Kovacevic, J. Berndt, T. Strunskus, L. Boufendi, *J. Appl. Phys.* **2012**, *112*, 013303.
- [35] M. Schulze, A. vonKeudell, P. Awakowicz, *Plasma Sources Sci. Technol.* **2006**, *15*, 556.
- [36] C. Hollenstein, *Plasma Phys. Control. Fusion* **2000**, *42*, R93.
- [37] S. Mitic, S. Coussan, C. Martin, L. Couëdel, *Plasma Processes Polym.* **2018**, *15*, 1700152.

How to cite this article: O. H. Asnaz, N. Kohlmann, H. Folger, F. Greiner, J. Benedikt. Growth and treatment of hydrogenated amorphous carbon nanoparticles in a low-pressure plasma *Plasma Processes Polym.* **2022**;19:e2100190. <https://doi.org/10.1002/ppap.202100190>